

# Using Zero Padding for Robust Channel Estimation in SEFDM Systems

Waseem Ozan, Ryan Grammenos and Izzat Darwazeh

Department of Electronic and Electrical Engineering, University College London, London, UK, WC1E 6BT  
{w.ozan; r.grammenos; i.darwazeh}@ucl.ac.uk

**Abstract**—In spectrally efficient frequency division multiplexing (SEFDM) systems, the subcarrier spacing is compressed below the orthogonality limit, to enhance the bandwidth utilisation with respect to orthogonal frequency division multiplexing (OFDM). This gives rise to inter-carrier interference (ICI) between the subcarriers and the received pilots are affected by self-ICI combined with multipath effects. Therefore, channel estimation becomes more challenging. In this work, a novel frequency-domain channel estimation approach is proposed for SEFDM systems, which employs zero padding (ZP) instead of a cyclic prefix (CP) for the transmitted pilot symbols. Subsequently, the multipath components that appear in the ZP part are used to enhance channel estimation.

**Index Terms**—cyclic prefix, zero padding, guard interval, channel estimation, non-orthogonal, spectrally efficient, SEFDM.

## I. INTRODUCTION

In spectrally efficient frequency division multiplexing (SEFDM) systems, the spacing between subcarriers is compressed below the Nyquist limit. Unlike orthogonal frequency division multiplexing (OFDM), SEFDM is a non-orthogonal scheme, which packs more subcarriers into the same spectrum relative to OFDM, thereby improving spectral efficiency [1]. SEFDM's ability to save spectrum makes it a topic of current interest, as exemplified by the great deal of work that is being carried out, by different research groups, in this field [2]–[7].

In addition, SEFDM has been implemented successfully in various communication systems, such as long-term evolution (LTE) [8], visible light communication (VLC) [9] and optical communication systems [10]. More recently, SEFDM signal modulation is used in vehicular communication systems [11], with bandwidth savings ranging from 20% to 60%. Such savings could be utilised to increase the number of users or improve data rate in future vehicular communication systems.

In SEFDM, channel estimation becomes more challenging due to combined self-created ICI and multipath effects. In [12] and [9], channel estimation was carried out in the time-domain. It has been shown that time-domain channel estimation techniques provide a good estimate, and subsequently, a good equalisation of the channel [8]. In addition, partial channel estimation (PCE) is used to enhance the channel estimation in the time-domain, where only the orthogonal subcarriers are used for estimation [12]. However, the computational complexity is relatively high since time-domain estimation requires at least one matrix inversion operation to perform the de-convolution process needed to estimate the channel. In

principle, the same performance should be achievable in the frequency-domain.

Xu [8], reports that the mean-square error (MSE) reaches an error floor at high  $E_b/N_o$  values, when channels are estimated using SEFDM pilots with a cyclic prefix (CP). The work in optical SEFDM [10] uses OFDM pilot symbols to estimate the channel. This is followed by an interpolation process of the estimated channel state information (CSI), which is used to compute the CSI for the compressed subcarriers in SEFDM signals. More recently, a new method utilising OFDM symbols was used to estimate channel characteristics [13], which was experimentally validated in [6], [14]. In this technique, a pilot OFDM symbol is sent at the start of every frame followed by SEFDM data symbols. However, the OFDM symbols are longer in the time domain compared to SEFDM symbols, hence, modifications to the standard resource blocks, such as LTE resource blocks, are needed.

This paper introduces a novel frequency-domain channel estimation technique employing zero padding (ZP) which is designed for non-orthogonal SEFDM systems. Muquet et al [15] provided a comprehensive review of the trade-offs associated with the use of a CP versus ZP in OFDM systems and concluded that in specific cases ZP has advantages over CP. The work in [16] proves analytically that using ZP in SEFDM decomposes the wideband channel onto a number of orthogonal narrowband subchannels. In this work, the CP is replaced by a ZP in SEFDM systems. We argue and show that ZP-SEFDM has two key advantages over CP-SEFDM; firstly, providing more information about the received multipath components at the receiver and second, the ZP part of the signal is free from the effects of the self-induced ICI present normally in SEFDM signals. Subsequently, the SEFDM pilot symbol plus the multipath components in the ZP part are used in the channel estimation process. These two factors improve the accuracy of the channel estimates. The validity of the theoretical findings is confirmed through extensive numerical simulations.

The remainder of this paper is organised as follows; Section II provides an overview of the SEFDM signal model. Section III presents the mathematical analysis using both a CP and a ZP in SEFDM systems. The proposed channel estimation technique for SEFDM system is described in Section IV. Simulation results are shown in Section V while Section VI concludes this paper.

## II. SEFDM SIGNAL MODEL

The SEFDM signals consist of a stream of symbols, where each symbol carries  $N$  complex symbols. Each complex symbol is modulated onto one subcarrier. Using the same number of subcarriers,  $N$ , SEFDM offers a bandwidth saving equal to  $((1-\alpha) \times \text{total bandwidth})$  in Hz compared to OFDM at the same transmission speed, where  $\alpha$  is the bandwidth compression factor. The discrete time-sampled SEFDM symbol is expressed as:

$$x(k) = \frac{1}{\sqrt{Q}} \sum_{n=0}^{Q-1} s_n e^{(j2\pi n k / Q)} \quad (1)$$

where  $k = [0, 1, 2, \dots, Q-1]$  is the index of the time samples in an SEFDM symbol,  $Q = \rho N$  and  $\rho$  is the oversampling rate and  $s_n$  is the complex symbol modulated on the  $n^{\text{th}}$  subcarrier.

Moreover, the discrete SEFDM pilot symbol can be given in matrix form as [16]:

$$\mathbf{x} = \Phi \mathbf{s} \quad (2)$$

where  $\mathbf{x}$  represents a  $Q$ -dimensional vector of a sampled SEFDM symbol in the time-domain,  $\mathbf{s}$  is an  $N$ -dimensional vector of a sampled input pilot signal in the frequency-domain and  $\Phi$  is a  $Q \times N$  matrix representing the sampled carrier matrix. The matrix elements of  $\Phi$  are given by  $\Phi_{k,n} = \frac{1}{\sqrt{Q}} \exp(j2\pi n k / Q)$ .

### III. ANALYSIS: CP AND ZP IN SEFDM SYSTEMS

The lack of orthogonality in SEFDM systems, leads to such signals having a non-integer number of cycles and a non-continuous phase between the CP and the SEFDM symbols, as depicted in Fig. 1. Hence, this work proposes the use of ZP in a novel way to improve the accuracy of the channel information obtained. The SEFDM symbol is first padded with zeros instead of using a CP. Subsequently, this extended time-domain signal is linearly convolved with the channel response. At the receiver, the extended signal is demodulated and the additional information appearing in the zero padding portion is utilised to improve the channel estimation accuracy. This process is illustrated in Fig. 2. The above concepts are mathematically analysed and validated in the following subsections.

#### A. Using Cyclic Prefix with SEFDM

Using the conventional technique, a CP part, which has  $L$  samples, is added at the beginning of each transmitted SEFDM pilot symbol, as shown in Fig. 1. The SEFDM pilot signals are transmitted through a wireless fading channel with channel impulse response denoted by  $h = [h_0, h_1, \dots, h_L]$ . At the receiver, the signal will arrive having been distorted by the channel and contaminated with additive white Gaussian noise (AWGN). Having removed the CP, the demodulated CP-SEFDM signal,  $\tilde{\mathbf{r}}_{cp}$ , is thereby expressed in vector form as [16]:

$$\tilde{\mathbf{r}}_{cp} = \lambda \odot \tilde{\mathbf{s}} + \tilde{\mathbf{r}}_{cp2} - \tilde{\mathbf{r}}_{cp3} + \tilde{\mathbf{z}}_{cp} \quad (3)$$

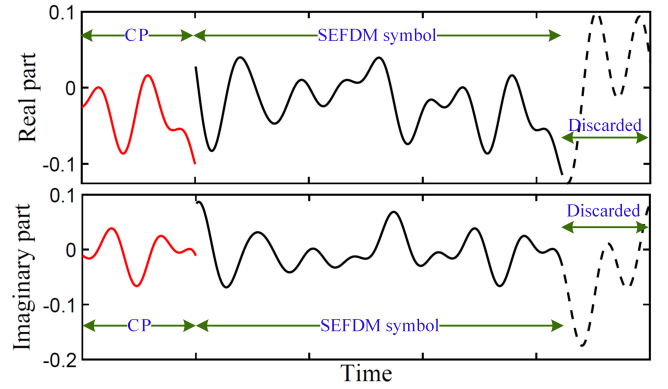


Fig. 1. Time samples of the real and imaginary parts of one CP-SEFDM symbol. The red curves are the guard interval parts while the black parts are the IDFT output. The solid-black curves are the SEFDM symbols and the dashed-black curves are the discarded samples at the output of the IDFT.

where  $\lambda$  is a vector of the narrowband subchannel gains,  $\tilde{\mathbf{s}} = \Gamma \mathbf{s}$  is the expected received SEFDM symbol when no multipath or noise channels are present,  $\Gamma = \Phi^H \Phi$  is the SEFDM correlation matrix, which quantifies the interference contribution to each subcarrier from its neighboring subcarriers [17],  $\tilde{\mathbf{z}}_{cp}$  refers to the AWGN noise vector, and the notation  $(\odot)$  is the element-wise multiplication. It should be evident that even in the absence of noise, the demodulated CP-SEFDM signal would comprise interference components from the missing and unwanted signals,  $\tilde{\mathbf{r}}_{cp2}$  and  $\tilde{\mathbf{r}}_{cp3}$ , respectively.

*Channel Estimation in CP-SEFDM:* The CP-SEFDM analytical expression of channel estimation is found using zero forcing and it is given by [16]:

$$\begin{aligned} \hat{\lambda} &= \tilde{\mathbf{r}}_{cp} ./ \tilde{\mathbf{s}} = (\lambda \odot \tilde{\mathbf{s}} + \tilde{\mathbf{r}}_{cp2} - \tilde{\mathbf{r}}_{cp3} + \tilde{\mathbf{z}}_{cp}) ./ \tilde{\mathbf{s}} \\ &= \underbrace{\lambda}_1 + \underbrace{\tilde{\mathbf{r}}_{cp2} ./ \tilde{\mathbf{s}}}_2 - \underbrace{\tilde{\mathbf{r}}_{cp3} ./ \tilde{\mathbf{s}}}_3 + \underbrace{\tilde{\mathbf{z}}_{cp} ./ \tilde{\mathbf{s}}}_4 \end{aligned} \quad (4)$$

where part 1 represents the subchannel gain estimated at each subcarrier, parts 2 and 3 are the added interference, part 4 corresponds to the noise signal, and the division operator notation  $(./)$  between the two vectors, in equations (4) and (8), is the element-wise division.

The lack of orthogonality and continuity in SEFDM signals gives rise to self-created ICI in the SEFDM symbols. As a result, the use of circular convolution has a counterproductive effect. Unlike OFDM, the (deliberate) violation of orthogonality in SEFDM will have counterproductive effects on the pilot symbols used for channel estimation. Furthermore, the non-continuous phase CP in SEFDM signals will be spread by the multipath channel, resulting in inter-symbol interference (ISI). The pilot symbols will also suffer from the ICI stemming from the compressed spacing between the subcarriers. This in turn prevents the use of one-tap frequency-domain channel estimation, and hence there is a need to employ a more sophisticated receiver in order to estimate the CSI.

#### B. Using Zero Padding with SEFDM

In this work, each SEFDM transmitted symbol is padded with zeros instead of the CP portion at the beginning of

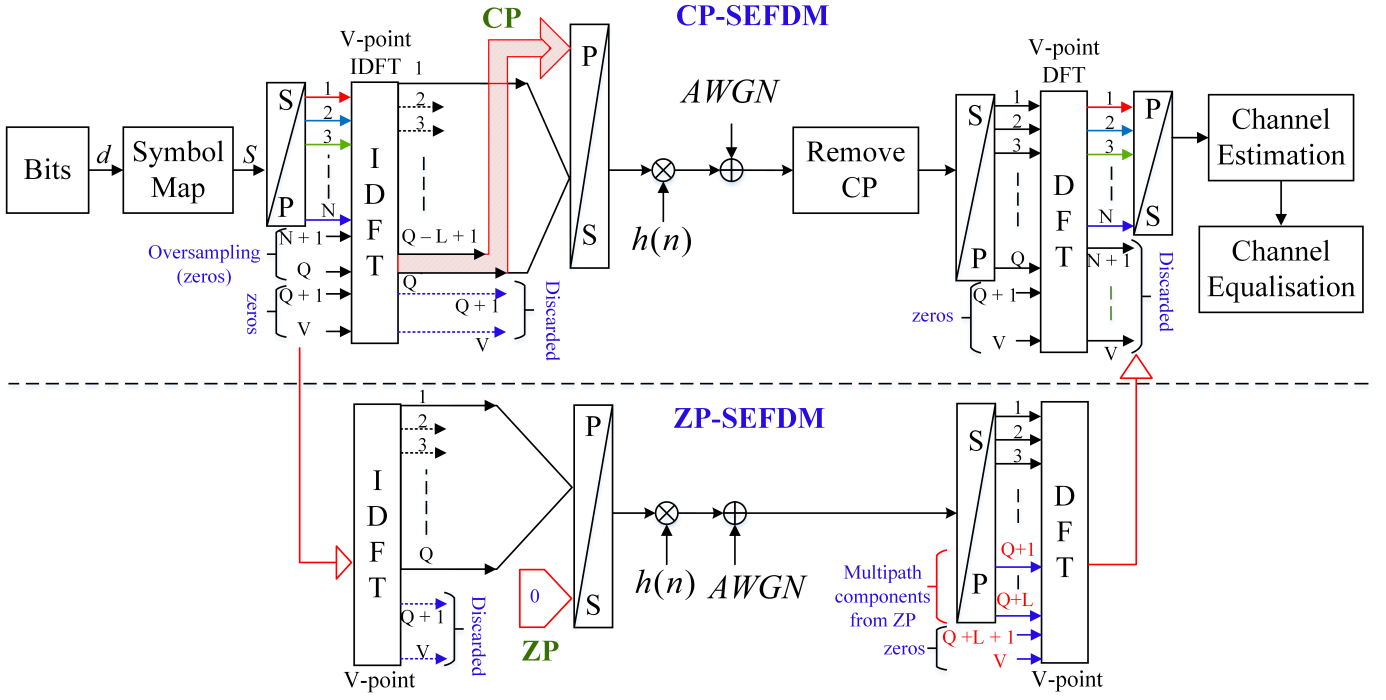


Fig. 2. Block diagram of a simplified SEFDM transceiver employing the proposed guard interval techniques for channel estimation. CP-SEFDM in the upper part, ZP-SEFDM in the lower part.

the symbols. The transmitted SEFDM symbols may then be represented as:

$$x'(k') = [x(0), x(1), \dots, x(Q-1), 0, 0, \dots, 0] \quad (5)$$

where the ZP part has the same length as the CP part.

Assuming this signal is transmitted through a multipath wireless channel, one received symbol will be given by:

$$y_{zp}(k') = h(k') * x'(k') + z(k') \quad (6)$$

where  $*$  denotes convolution and  $\mathbf{z}$  is the AWGN noise vector of the same size as  $\mathbf{y}_{zp}$ .

At the receiver, the SEFDM symbols, in which the ZP contains information about the energy spillage arising from ISI, are fed to a DFT, which has size  $V = Q/\alpha$ . In this scenario, the demodulated signal,  $\mathbf{r}_{zp}$ , is represented by [16]:

$$\mathbf{r}_{zp} = \boldsymbol{\lambda}_{zp} \odot \tilde{\mathbf{s}} + \tilde{\mathbf{z}}_{\Phi} \quad (7)$$

where  $\boldsymbol{\lambda}_{zp}$  is the subchannel gains vector and  $\tilde{\mathbf{z}}_{\Phi}$  is the  $V \times 1$  AWGN noise vector. Equation (7), provides evidence that using ZP instead of a CP in SEFDM allows the decomposition of the wideband multipath channel into independent narrowband channels.

*Channel Estimation in ZP-SEFDM:* The analytical expression of estimated channel characteristics for ZP-SEFDM are given by [16]:

$$\begin{aligned} \hat{\boldsymbol{\lambda}}_{zp} &= \mathbf{r}_{zp} \cdot \tilde{\mathbf{s}} \\ &= (\boldsymbol{\lambda}_{zp} \odot \tilde{\mathbf{s}} + \tilde{\mathbf{z}}_{\Phi}) \cdot \tilde{\mathbf{s}} = \underbrace{\boldsymbol{\lambda}_{zp}}_1 + \underbrace{\tilde{\mathbf{z}}_{\Phi} \cdot \tilde{\mathbf{s}}}_2 \end{aligned} \quad (8)$$

where part 1, describes the channel gains while part 2 corresponds to the noise vector.

It should be noted that the ZP is used with the SEFDM symbols to improve the channel estimation, where the ZP contains the pilot signal spread by the multipath channel but without the inherent ICI present in SEFDM signals, since the ZP is not an extension of the raw SEFDM signal (contrary to the case when utilising a CP).

#### IV. SYSTEM OPERATION

Fig. 2 depicts a simplified SEFDM transceiver for system testing. In this scenario, the guard interval (GI) length is selected in accordance with the LTE standards [18]. The only difference is that the CP employed in LTE is replaced by a ZP in this work.

At the transmitter, a stream of bits,  $d$ , is generated and mapped into quadrature phase shift keying (QPSK) symbols to generate the pilot symbols,  $S$ , where these symbols are known to both the transmitter and the receiver. The latter are input to an inverse discrete Fourier transform (IDFT), which is used to generate the non-orthogonal SEFDM signal; where a specified number of zeros are appended to the input of the IDFT, thus giving rise to  $V = Q/\alpha$  samples. Consequently, a  $V$ -point IDFT is required to generate the SEFDM signal of  $N$  active subcarriers, where the remaining  $V - N$  inputs are fed with zeros. Of these  $V - N$  zeros,  $(Q - N)$  zeros are introduced due to the oversampling ratio,  $\rho$ . The remaining  $(V - Q)$  zeros which are added to the input of the IDFT depend on the level of bandwidth compression applied. The same number of  $(V - Q)$  samples are discarded at the output of the IDFT, while the

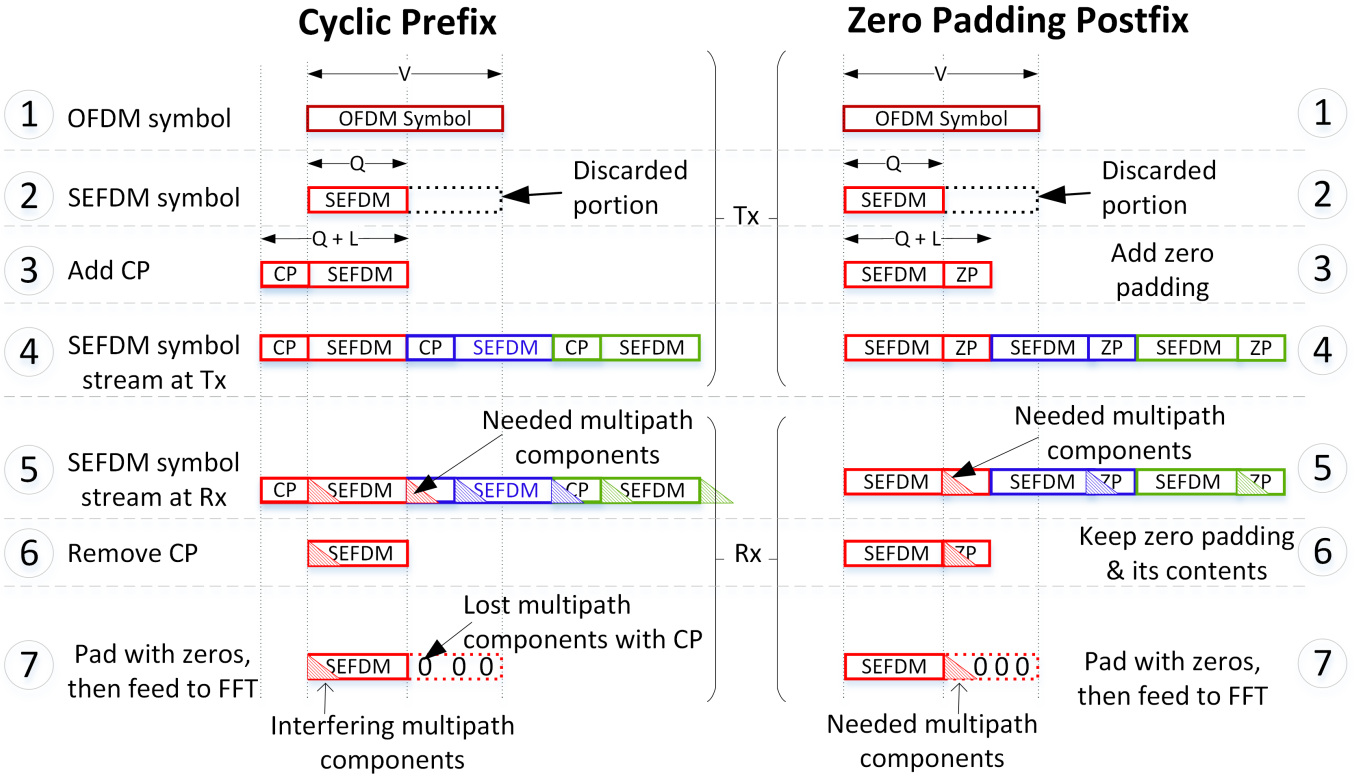


Fig. 3. Signals representation for the two systems tested in this work, CP-SEFDM and ZP-SEFDM.

$Q$  samples that are taken forward make up a single SEFDM symbol. This process may be understood better by referring to Fig. 3, specifically steps 1 and 2. The remaining steps in Fig. 3 (steps 3 to 7) illustrate the differences between the utilisation of a CP versus a ZP postfix when applied to a raw SEFDM data symbol.

#### A. CP-SEFDM

The upper part of Fig. 2 depicts the CP-SEFDM system. In which, a CP, of length  $L$ , is added at the beginning of every SEFDM symbol before the signal is transmitted through a wireless fading channel. Thus the number of time-domain samples of every transmitted SEFDM symbol is  $Q + L$ . At the receiver, the CP portion is discarded first and then, every SEFDM symbol is padded with zeros of length  $(V - Q)$ . The resulting signal is then fed to a DFT to convert the signal to the frequency-domain.

In order to fulfill the circular convolution criterion, two conditions must be obeyed. First, the signal plus the CP portion must be continuous in phase when they are transmitted through the wireless fading channel. Second, the input samples to the DFT should form a periodic signal. These two conditions are met in CP-OFDM signals. However, in CP-SEFDM signals, there is a discontinuity in phase between the CP portion and the SEFDM symbol [13], which leads to interference being introduced from the CP to the SEFDM symbol. In addition, after removing the CP portion at the receiver, the SEFDM

symbols are padded with zeros at the input of the DFT, which in turn yields a non-continuous signal in the time-domain, hence introducing additional interference to the subcarriers. As a result of the aforementioned reasons, inaccurate channel estimation and hence inaccurate channel equalisation occur in CP-SEFDM systems, as depicted in steps 5-7 in Fig. 3.

#### B. ZP-SEFDM

The lower part of Fig. 2 depicts the ZP-SEFDM system, in which the CP is replaced by trailing zeros of length  $L$  that are attached to the end of each SEFDM symbol. The SEFDM symbols including the ZP arrive at the receiver distorted by the multipath channel and contaminated with AWGN; where the power within the ZP is no longer equal to zero, due to the spillage of energy in the SEFDM pilot symbols caused by the multipath channel. The SEFDM symbols plus the ZP portion are fed to a DFT to convert the signal to the frequency-domain. Due to the fact that the ZP portion comprises only null samples, ZP-SEFDM eliminates the multipath components stemming from the discontinuous CP in CP-SEFDM. Instead, these multipath components appear in the ZP portion of the signal, as illustrated in step 7 of Fig. 3 (on the right-hand-side). Hence, the received ZP-SEFDM signal essentially represents a linear convolution of the transmitted ZP-SEFDM signal with the channel impulse response. The output of this linear convolution is fed to a DFT at the receiver. The result are SEFDM subcarriers with flat channel gain associated with

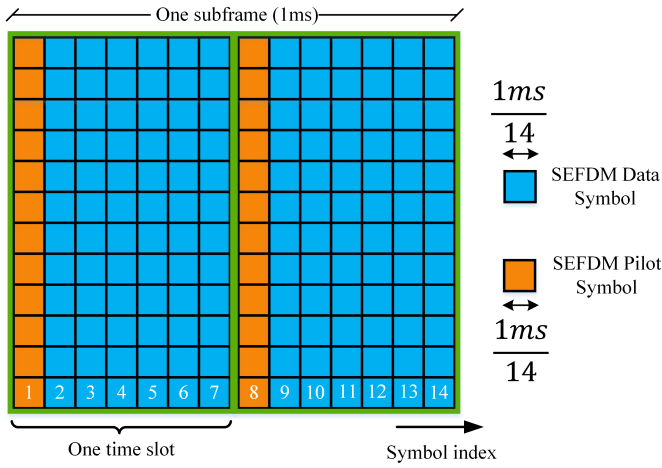


Fig. 4. Frame structure.

TABLE I  
CHANNEL MODEL PARAMETERS

Parameters	Value
Channel delay profile	TDL-D
Delay spread	300 ns
Maximum Doppler shift	111.2 Hz
K-factor	7 dB

each subcarrier. Therefore, one-tap channel estimation and equalisation can be performed without additional interference coming from the CP, and hence, ZP-SEFDM outperforms CP-SEFDM with respect to obtaining accurate channel estimation.

## V. SYSTEM PARAMETERS AND RESULTS

System parameters in the computer simulations are carried out based on the narrowband internet-of-things (NB-IoT) standard [19]. The NB-IoT system parameters are appropriately modified to accommodate the bandwidth compression factors ranging between  $\alpha = 0.5 - 0.9$  [16], [20], [21]. The system parameters are:  $N = 12$  data subcarriers,  $Q = 128$  [20] and the modulation format is quadrature phase shift keying (QPSK) [16].

The frame structure is similar to that in LTE [19] where every radio frame of length 10 ms consists of ten equally sized subframes, each of which contains  $2 \times 0.5$  ms time slots. In every time slot, there are seven SEFDM symbols. Of these seven symbols, one carries a pilot, which is used for channel estimation, while the other six symbols carry data signals. The pilot symbols are the demodulation reference symbol (DMRS) [19]. Fig. 4 depicts the frame structure used in this simulation evaluation.

The MSE in channel estimation, error vector magnitude (EVM) and bit error rate (BER) are computed for both CP-SEFDM and ZP-SEFDM systems using 5G-new radio (5G-NR) tapped delayed line (TDL) channel model of type (D). The tap delays and power values are given in Table 7.7.2-4 of the standards [22] and the channel model parameters are given in Table I here.

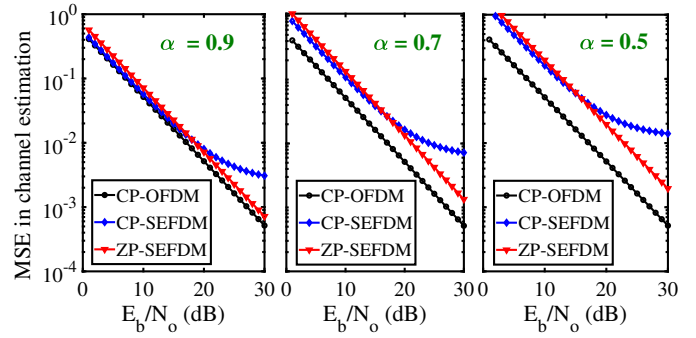


Fig. 5. MSE results using TDL-D channel model.

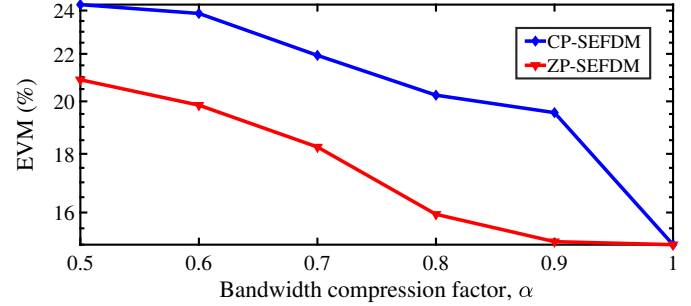


Fig. 6. EVM results using TDL-D channel model.

Fig. 5 compares the MSE of SEFDM systems employing a CP or a ZP for different values of the compression factor,  $\alpha = 0.9, 0.7$  and  $0.5$ . The figures show that, when CP-SEFDM fails to estimate the channel resulting in high MSE values, the new technique estimates well, for low and high values of  $E_b/N_o$ . From the figures, it can be inferred that the MSE of the CP-based channel estimation in SEFDM systems eventually reaches a non-zero error floor level for any value of  $\alpha < 1$ . On the contrary, the MSE for the ZP method is monotonically decreasing.

To better evaluate ZP-SEFDM versus CP-SEFDM systems, EVM is examined for both systems after channel equalisation process using the estimated channel characteristics via ZP-SEFDM and CP-SEFDM pilots. EVM is the chosen figure-of-merit used here to evaluate the distortion in the complex received signal that affects signal reliability, where impairments are introduced by many factors, such as noise and amplitude distortion. In Fig. 6, EVM performances are depicted for different compression factors ranging from 1 to 0.5, using QPSK for modulation format and at  $E_b/N_o = 15$  dB. From the EVM plots, it is clear that ZP-SEFDM outperforms CP-SEFDM in the two channel scenarios as the ZP-SEFDM has lower EVM values because no distortion is introduced by the discontinuous CP portion in SEFDM systems. As expected, Fig. 6 shows that higher spectral efficiencies (lower  $\alpha$  values) come at the expense of signal deterioration, which is apparent in terms of worse EVM values due to higher levels of self-generated ICI.

Moreover, the frequency-domain channel estimation and equalisation methods in SEFDM systems reduce the computational complexity in comparison to time-domain ones with similar performance to the results presented in [8]. The reason behind this is that time-domain estimation/equalisation requires matrix inversion, where the computational complexity increases exponentially with the number of subcarriers,  $N$ , while for frequency-domain methods, only one simple division process is required for each of the channel estimation and equalisation processes and where the computational complexity increases linearly by  $N$ .

The proposed ZP method in SEFDM systems shows the advantage in channel estimation, thus paving the way for the practical use of ZP-SEFDM in vehicular communication systems. In addition, following the use of ZP instead of CP in SEFDM systems, ZP can be similarly employed in other non-orthogonal signals to gain the same advantages in improving the channel estimation and hence obtaining more accurate channel equalisation performance as in the SEFDM ones. Such non-orthogonal signals and systems are faster-than-Nyquist (FTN) [23], [24], Truncated OFDM (TOFDM) [25], [26] and generalised frequency division multiplexing (GFDM) [27].

## VI. CONCLUSION

The deliberate violation of the orthogonality rule in SEFDM systems leads to self-induced ICI between the subcarriers. Therefore, the received pilots are affected by both the self-ICI, as well as ISI resulting from the multipath channel. The use of a conventional CP in SEFDM systems mitigates ISI at low  $E_b/N_o$ , however, the inaccuracy in channel estimation performance reaches a non-zero error floor for higher values.

To address this issue, a novel frequency-domain channel estimation technique for SEFDM systems utilising ZP instead of a CP was proposed in this work. It is shown that the proposed technique improves channel estimation and thus leads to better equalisation accuracy. The ZP is used with the pilot symbols to enhance the channel state information acquired at the receiver. Simulation results show that the MSE can be improved by over one order of magnitude at high  $E_b/N_o$  values when the ZP-based technique is used instead of a CP.

## REFERENCES

- [1] I. Kanaras, A. Chorti, M. R. D. Rodrigues, and I. Darwazeh, "Spectrally Efficient FDM Signals: Bandwidth Gain at the Expense of Receiver Complexity," in *Proc. IEEE Int. Conf. Commun.*, June 2009, pp. 1–6.
- [2] D. Rainnie *et al.*, "On capacity merits of spectrally efficient FDM," in *2015 IEEE Military Commun. Conf.*, Oct 2015, pp. 581–586.
- [3] S. V. Zavjalov, S. V. Volvenko, and S. B. Makarov, "A Method for Increasing the Spectral and Energy Efficiency SEFDM Signals," *IEEE Commun. Lett.*, vol. 20, no. 12, pp. 2382–2385, Dec 2016.
- [4] K. Park *et al.*, "Iterative frequency-domain inter-carrier interference cancellation for coded SEFDM," *Electronics Lett.*, vol. 53, no. 19, pp. 1333–1335, 2017.
- [5] B. Yu *et al.*, "Channel equalisation and data detection for SEFDM over frequency selective fading channels," *IET Commun.*, vol. 12, no. 18, pp. 2315–2323, 2018.
- [6] W. Ozan *et al.*, "Experimental SEFDM Pipelined Iterative Detection Architecture with Improved Throughput," in *2018 IEEE 87th Vehicular Technol. Conf. (VTC Spring)*, June 2018, pp. 1–5.

- [7] M. Jia, Z. Yin, Q. Guo, G. Liu, and X. Gu, "Downlink design for spectrum efficient IoT network," *IEEE Internet of Things Journal*, vol. 5, no. 5, pp. 3397–3404, 2017.
- [8] T. Xu and I. Darwazeh, "Transmission Experiment of Bandwidth Compressed Carrier Aggregation in a Realistic Fading Channel," *IEEE Trans. Veh. Technol.*, vol. 66, no. 5, pp. 4087–4097, May 2017.
- [9] Y. Wang *et al.*, "SEFDM Based Spectrum Compressed VLC System Using RLS Time-domain Channel Estimation and ID-FSD Hybrid Decoder," in *Proc. 42nd European Conf. on Opt. Commun. (ECOC)*, Sep. 2016, pp. 1–3.
- [10] D. Nopchinda *et al.*, "Dual Polarization Coherent Optical Spectrally Efficient Frequency Division Multiplexing," *IEEE Photonics Tech. Lett.*, vol. 28, no. 1, pp. 83–86, Jan 2016.
- [11] S. Stainton *et al.*, "Neural Network Equalisation and Symbol Detection for 802.11p V2V Communication at 5.9GHz," in *2020 IEEE 91st Vehicular Technology Conference (VTC Spring)*. IEEE, 2020.
- [12] S. Isam and I. Darwazeh, "Robust channel estimation for Spectrally Efficient FDM system," in *Proc. 19th Int. Conf. Telecommun. (ICT)*, April 2012, pp. 1–6.
- [13] H. Ghannam and I. Darwazeh, "Robust Channel Estimation Methods for Spectrally Efficient FDM Systems," in *Proc. IEEE 87th Veh. Technol. Conf. (VTC Spring)*, June 2018, pp. 1–6.
- [14] W. Ozan, H. Ghannam, T. Xu, P. A. Haigh, and I. Darwazeh, "Experimental Evaluation of Channel Estimation and Equalisation in Non-Orthogonal FDM Systems," in *2018 11th International Symposium on Communication Systems, Networks & Digital Signal Processing (CSNDSP)*. IEEE, 2018, pp. 1–6.
- [15] B. Muquet, Zhengdao Wang, G. B. Giannakis, M. de Courville, and P. Duhamel, "Cyclic prefixing or zero padding for wireless multicarrier transmissions?" *IEEE Trans. Commun.*, vol. 50, no. 12, pp. 2136–2148, Dec 2002.
- [16] W. Ozan, R. Grammenos, and I. Darwazeh, "Zero padding or cyclic prefix: Evaluation for non-orthogonal signals," *IEEE Communications Letters*, 2020.
- [17] S. Isam *et al.*, "Characterizing the intercarrier interference of non-orthogonal Spectrally Efficient FDM system," in *2012 8th Int. Symp. Commun. Syst., Netw. Digit. Signal Process. (CSNDSP)*, July 2012, pp. 1–5.
- [18] G. T. version 8.12.0 Release 8, "Evolved universal terrestrial radio access (E-UTRA) and evolved universal terrestrial radio access network (EUTRAN); overall description; stage 2 (release 8)," April 2010.
- [19] 3GPP, "LTE; Evolved Universal Terrestrial Radio Access; Physical layer procedures," 3GPP, TS 36.213, Rel. 14, v.14.2.0, Apr. 2017.
- [20] T. Xu, C. Masouros, and I. Darwazeh, "Waveform and Space Precoding for Next Generation Downlink Narrowband IoT," *IEEE Internet Things J.*, vol. 6, no. 3, pp. 5097–5107, June 2019.
- [21] W. Ozan *et al.*, "Time Precoding Enabled Non-Orthogonal Frequency Division Multiplexing," in *Proc. 30th IEEE Int. Symp. on Personal, Indoor and Mobile Radio Communications*, Sep. 2019, pp. 1–6.
- [22] 3GPP, "5G; Study on channel model for frequencies from 0.5 to 100 GHz," 3GPP, TR 38.901, Rel. 14, v.14.0.0, May 2017.
- [23] F. Rusek and J. B. Anderson, "Multistream faster than Nyquist signaling," *IEEE Transactions on Communications*, vol. 57, no. 5, pp. 1329–1340, 2009.
- [24] S. Sugiura, "Frequency-domain equalization of faster-than-Nyquist signaling," *IEEE Wireless Communications Letters*, vol. 2, no. 5, pp. 555–558, 2013.
- [25] W. Ozan, K. Jamieson, and I. Darwazeh, "Truncating and oversampling OFDM signals in white Gaussian noise channels," in *2016 10th International Symposium on Communication Systems, Networks and Digital Signal Processing (CSNDSP)*. IEEE, 2016, pp. 1–6.
- [26] M. Jia, Z. Yin, D. Li, Q. Guo, and X. Gu, "Toward improved offloading efficiency of data transmission in the IoT-cloud by leveraging secure truncating OFDM," *IEEE Internet of Things Journal*, vol. 6, no. 3, pp. 4252–4261, 2018.
- [27] N. Michailow, M. Matthé, I. S. Gaspar, A. N. Caldevilla, L. L. Mendes, A. Festag, and G. Fettweis, "Generalized frequency division multiplexing for 5th generation cellular networks," *IEEE Transactions on Communications*, vol. 62, no. 9, pp. 3045–3061, 2014.